Proton Irradiation of High Aluminum Content AlGaN Polarization Doped Field Effect Transistors

ECS Journal of Solid State Science and Technology, 2020 **9** 025003
2162-8777/2020/9(2)/025003/6/$40.00 © 2020 The Electrochemical Society ("ECS"). Published on behalf of ECS by IOP Publishing Limited

Proton Irradiation of High Aluminum Content AlGaN Polarization Doped Field Effect Transistors

Patrick H. CareyIV,[1,*,z] Fan Ren,[1,] Jinho Bae,[2] Jihyun Kim,[2,***] and Stephen J. Pearton[3,**]**

[1]*Department of Chemical Engineering, University of Florida, Gainesville, Florida 32608, United States of America*
[2]*Department of Chemical and Biological Engineering, Korea University, Seoul 02841, Republic of Korea*
[3]*Department of Material Science and Engineering, University of Florida, Gainesville, Florida 32608, United States of America*

The effects of proton irradiation dose on the DC and switching properties of high aluminum content, polarization-doped field effect transistors (POLFETs) were studied. The POLFETs were irradiated at proton energy of 10 MeV at fluences of 1×10^{14} cm^{-2} and 3×10^{14} cm^{-2}. The DC saturation current exhibited a 21 and 36% reduction at fluences of 1×10^{14} cm^{-2} and 3×10^{14} cm^{-2}, respectively. The carrier removal rates for this energy was 677 cm^{-1}. However, switching current at 100 kHz demonstrated no change, with near ideal performance, as opposed to significant degradation in their GaN HEMT counterparts. This near ideal performance is attributed to the volume of the 3D electron gas in the POLFETs reducing the likelihood of negatively impacting scattering events, as opposed to the narrow 2D electron gas of the HEMT. The DC degradation and carrier removal rates are on par with reported traditional GaN HEMTs, but the switching performance is exceptionally improved.
 [DOI: 10.1149/2162-8777/ab71f0]

Manuscript submitted December 12, 2019; revised manuscript received January 28, 2020. Published February 10, 2020.

Spacecraft are subject to significant environmental damage by various fluxes of high energy radiation that make design and implementation more difficult than their permanently terrestrial operating counterparts. One of the most challenging aspects for electronic design is providing sufficient radiation protection to sensitive electronic components at the tradeoff of a higher weight and higher cost for heavier payloads. For low earth orbit (LEO), the primary radiation source are the Van Allen radiation belts, which were discovered when the Explorer I and Explorer III Geiger counters saturated from high radiation flux.[1] The Van Allen belts are primarily composed of low energy ($\leqslant$10 MeV) protons and electrons which are trapped by the Earth's magnetic field in a toroidal circuit. Other sources of radiation include cosmic rays and single solar events. The former providing fairly low energy radiation $<$ 100 keV, while single solar events occur on the cycles of four inactive years of low annual fluence, followed by seven active years with fluences above 5×10^7 particles cm^{-2} at energies $>$ 10 MeV.[2]

In order to extend the lifetime of space-bound microelectronics, aluminum shielding is commonly used; however, that adds mass to the spacecraft that could have been used for other instrumentation. Alternatively, shifting to radiation hard materials can reduce the need for shielding. The shift from GaAs to GaN led to an approximate improvement of 1000% improvement in radiation resistance.[3–9] While the bond energy of Ga-As is only 2.17 eV, the bond strength of Ga-N is 9.12 eV. This 4 fold increase in bond strength is not proportionally reflected in the performance improvement, the remainder is likely due to the piezoelectric field at the channel barrier layer interface of AlGaN/GaN reinjecting scattered carriers into the 2DEG.[9] To improve further upon GaN-based devices, the next shift is to ultrawide bandgap materials such as high aluminum content AlGaN. The primary advantage of shifting to a material such as $Al_{0.7}Ga_{0.3}N$ with a bandgap of 5.4 eV is the improvement in high voltage applications, with early results already finding high critical electric fields for breakdown of 3.6 MV cm^{-1}.[10] Additionally, high temperature operation at 500 °C has been a focus of study with the devices operating with near-ideal characteristics at 100 kHz with full pinchoff.[11] The benefit of shifting from a heterojunction which was used in the aforementioned works, is that the POLFET avoids issues of interfacial roughness, simplifies Ohmic contact formation, and prevents carrier freeze-out at extreme low temperature operation.[12–14]

This polarization doped field effect transistor has been previously well-characterized with elucidation on band structure and fabrication in an earlier work.[15] In this current work, a comparison to traditional GaN HEMT devices will be drawn to demonstrate the potential for high Al-content POLFETs and their improved radiation hardness. Only one previous report explored the effects of heavy ion radiation and brief proton irradiation on high aluminum content AlGaN HEMT structures, so much further work needs to be performed to define the potential of these devices.[16] No work has been reported for radiation damage studies on their POLFET counterparts. In this paper, DC characterization and medium frequency switching were performed to identify degradation in high Al content POLFETs from proton irradiation at 10 MeV and fluences of 1×10^{14} cm^{-2} and 3×10^{14} cm^{-2}.

Experimental

The POLFET structures were grown by metal organic vapor phase epitaxy on (0001) c-plane sapphire substrates mis-oriented by 0.2° toward the *m*-plane using trimethylgallium, trimethylammonia, and ammonia as precursors. A thick AlN nucleation and buffer layer of 2.3 μm was grown, followed by 0.25 μm unintentionally doped $Al_{0.7}Ga_{0.3}N$. A linear grade from 0.7 to 0.85 content aluminum was grown over 110 nm. Contactless mercury probe measurements yielded a sheet resistance of 5500 Ω/□ and a sheet carrier density of 5.4×10^{12} cm^{-2}. Circular POLFETs with a gate length of 3 μm and source/drain to gate distance of 3.5 μm were fabricated. The gate circumference was 660 μm. Planar Ohmic contacts were deposited by electron beam deposition (Zr/Al/Mo/Au) and annealed ($\rho_c = 1.1 \times 10^{-3}$ Ω-cm^{-2}). The gate (Ni/Au) was deposited through an opening in the PECVD deposited SiN_x passivation. A schematic of the final device structure is shown in Fig. 1. Three devices per irradiation condition were tested.

DC characterization was performed using an Agilent 4156 C Semiconductor Parameter Analyzer. Pulsed characteristics were captured using an Agilent DSO7054B oscilloscope with a DC power supply, Hewlett-Packard E3615A and an Agilent B114A Pulse Generator. Capacitance Voltage (C-V) characteristics were recorded with an Agilent 4284 A Precision LCR Meter.

Proton irradiation was performed at the Korean Institute of Radiological and Medical Sciences using a Scanditronix MC 50 cyclotron. The proton energy leaving the cyclotron was 30 MeV and adjusted to reach the samples at 10 MeV by using the appropriate

*Electrochemical Society Student Member.
**Electrochemical Society Fellow.
***Electrochemical Society Member.
[z]E-mail: careyph@ufl.edu

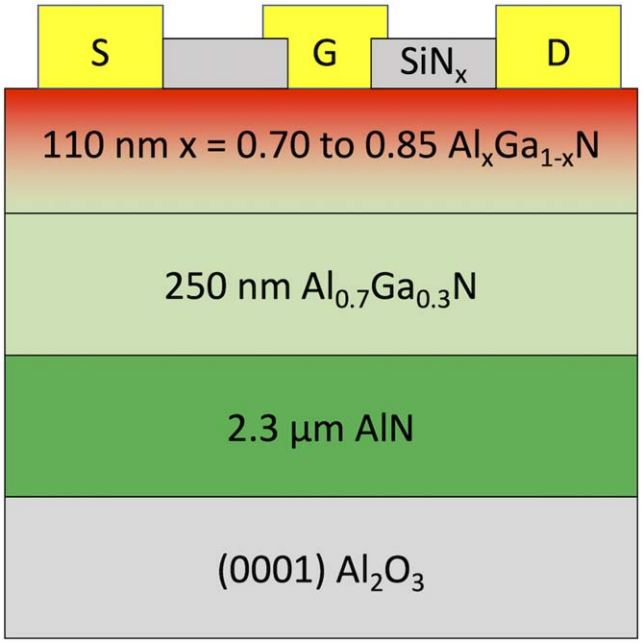

Figure 1. POLFET device schematic.

aluminum degraders. The irradiation was performed at two fluences, 1×10^{14} cm^{-2} and 3×10^{14} cm^{-2}, with the beam current being monitored through a Faraday cup to calculate the flux density. Samples were irradiated simultaneously from the front side after mounting to a carrier.

Stopping and Range of Ions in Matter (SRIM) simulations were performed to assess the electronic and nuclear stopping forces on the proton as it traversed through the devices.

Results and Discussion

The interaction of energetic protons incident upon and traversing a material are a combination of several key scattering events. At sufficiently high energies, the proton has a relatively straight path through the material, mainly losing energy as the charge of the proton interacts with electron orbitals of the material, so-called electronic energy loss. The other energy loss mechanism is collisions with, or scattering from, the nuclei of the target material, labelled nuclear stopping. This interaction will provide the majority of the energy loss for the proton at lower energies, producing the total displacement damage (TDD). As it traverses the material, the proton can ionize the medium and contribute to the Total Ionizing Dose (TID), by which degradation of the device is proportional to the received dose. Single Event Effects (SEE) are permanent effects due to a single transient particle inducing device damage, such as creating a short between gate and source.

To further understand the displacement and ionization energy losses per unit path length within our devices, SRIM calculations were performed to compare the electronic and nuclear stopping forces within key alloys of AlGaN used in the devices. These calculations are summarized in Fig. 2. The effects of nuclear energy loss are nearly linear with proton energy on a log-log scale, but the ionizing losses demonstrate a maximum, which arises from considering that below a threshold energy, the straggle of the proton outside its original path becomes larger and is more apt to lose energy by nuclear stopping as it slows down. To understand the trend of the increasing aluminum content, we can turn to the Bethe formula, which describes the energy loss per distance by a fast-moving charged particle through a medium:

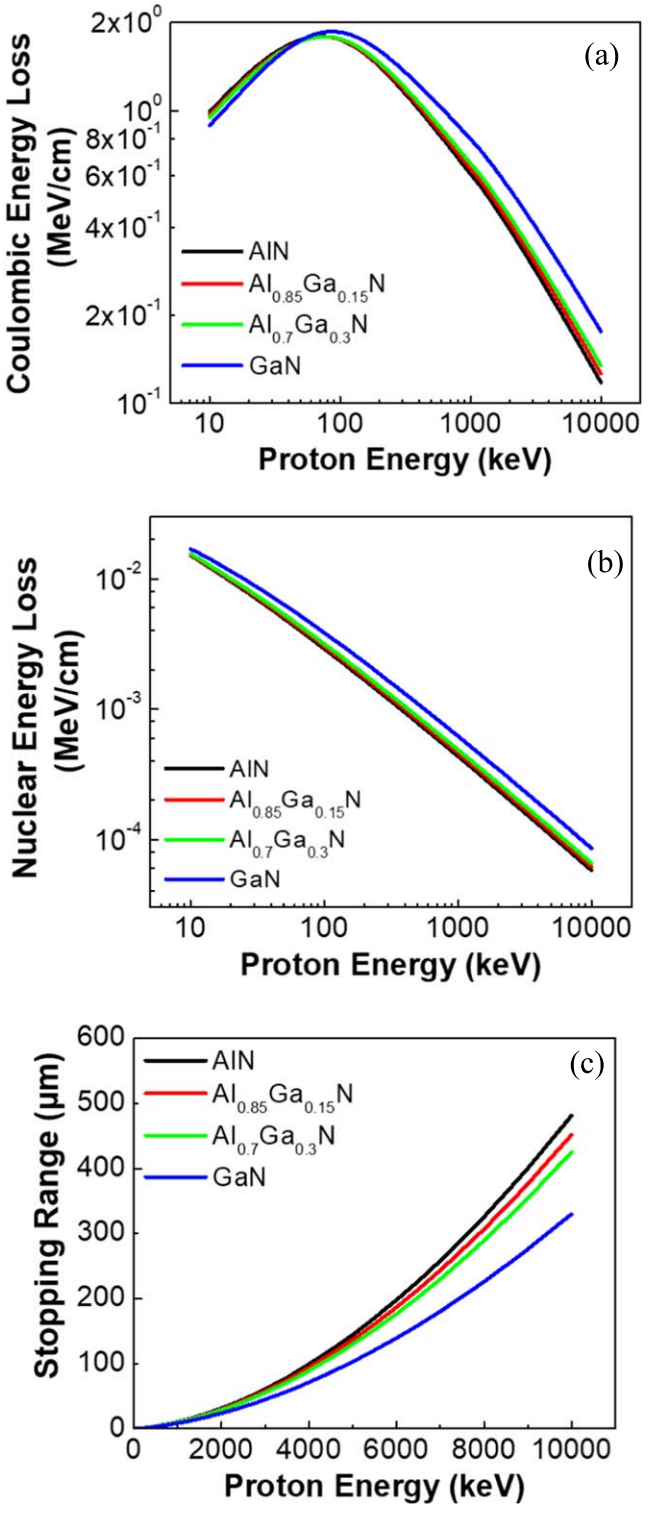

Figure 2. Stopping Range in Motion (SRIM) modeling of the (a) Coulombic energy loss and (b) Nuclear energy loss in GaN, $Al_{0.7}Ga_{0.3}N$, $Al_{0.85}Ga_{0.15}N$, and AlN.

$$-\frac{dE}{dx} = \frac{4\pi}{m_e} \cdot \frac{nz^2}{\beta^2} \cdot \left(\frac{q^2}{4\pi\varepsilon_0}\right)^2 \cdot \left[\ln\left(\frac{2m_e c^2\beta^2}{I \cdot (1-\beta^2)}\right) - \beta^2\right] \quad [1]$$

where E is energy, x is traveling distance into a target, n is target electron number density, I is mean excitation potential, q is electronic charge, m_e is the rest mass, z is the charge of the particle,

Table I. Material parameters for estimation of electron density in bulk material.

Parameter	GaN	AlN
Z (electrons)	38	20
ρ (g cm^{-3})	6.15	3.26
M (g mol^{-1})	83.73	40.98

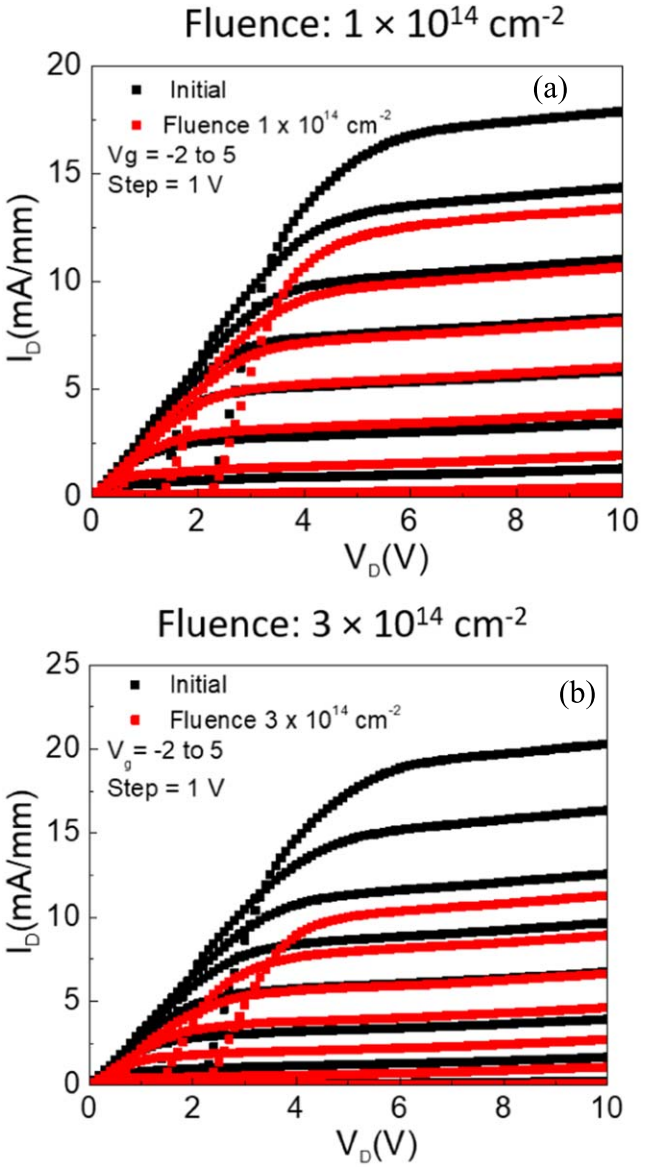

Figure 3. Current-voltage characteristics in the reference and fluences of (a) 1×10^{14} cm^{-2} and (b) 3×10^{14} cm^{-2}.

and $\beta = v/c$, where v is the particle speed, and c is the speed of light. The electron density of a material can be approximated by:

$$n = \frac{N_A \cdot Z \cdot \rho}{M} \quad [2]$$

where N_A is Avogadro's number, Z is the number of electrons per unit of the material, ρ is the density of the material, and M is the molecular mass of the material. If we calculate the electron density using the values in Table I, for GaN and AlN we find that n is approximately 1.68×10^{24} cm^{-3} and 9.58×10^{23} cm^{-3}, respectively. Since GaN has a higher electron density, it would be expected

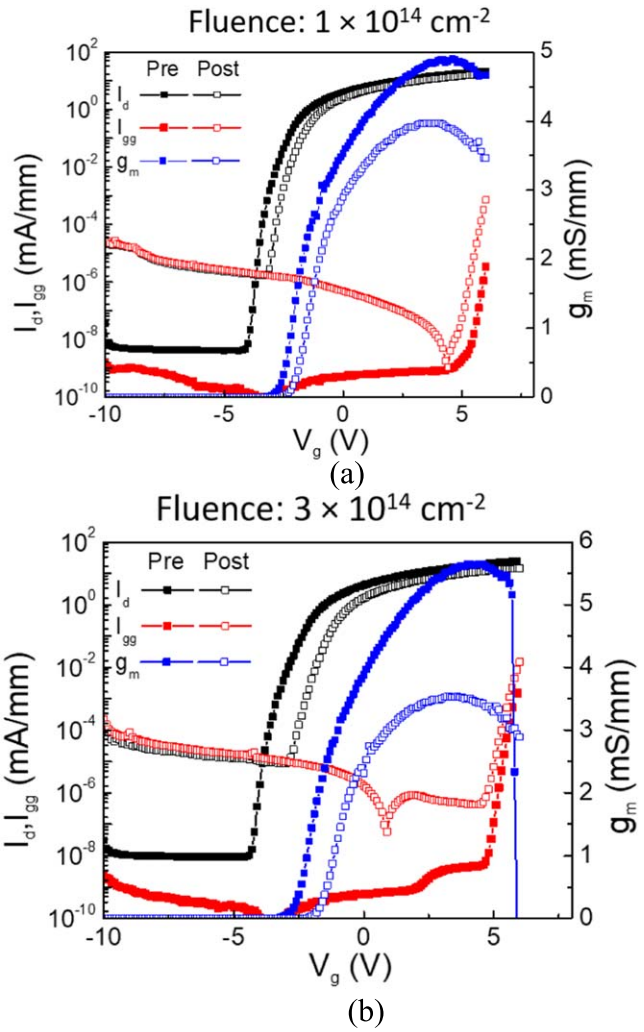

Figure 4. Drain current, gate current, and transconductance of the reference state and irradiated state POLFETs at fluences of (a) 1×10^{14} cm^{-2} and (b) 3×10^{14} cm^{-2}.

to undergo more ionization losses as more interactions can occur. As expected, more interactions lead to a shorter stopping distance in GaN, Fig. 2c. This approximation does have its limitations as it cannot account for a crystalline structure and the piezoelectric effect within our devices; however, it is still valuable as it presents an explicit relation of the key material parameters to the energy loss within the material.

From the modeled results, since GaN based devices should absorb more total energy loss, damage effects should be more prevalent and lead to a larger relative degradation over the AlGaN counterparts. Additionally, the bond strengths of Ga-N and Al-N, 8.92 eV atom^{-1} and 11.52 eV atom^{-1}, respectively, so the lower displacement damage expected demonstrates the potential for alloyed AlGaN over traditional GaN in space electronics subject to high radiation fluences.

In Fig. 3, current-voltage (I-V) characteristics are presented for a POLFET device before and after irradiation at a fluence of 1×10^{14} cm^{-2} and 3×10^{14} cm^{-2} at 10 MeV. The average drain saturation current was reduced by 24.3% ± 0.9% and 48% ± 4.1% at the doses of 1×10^{14} cm^{-2} and 3×10^{14} cm^{-2}, respectively. Beneath the knee voltage, the mobility of the electrons is proportional to their velocity as the electric field is insufficient to induce the saturation velocity, v_s. The slopes of the curves beneath the knee voltage has been reduced, which is indicative of loss of electron mobility as due to radiation induced scattering defects. Transfer characteristics are

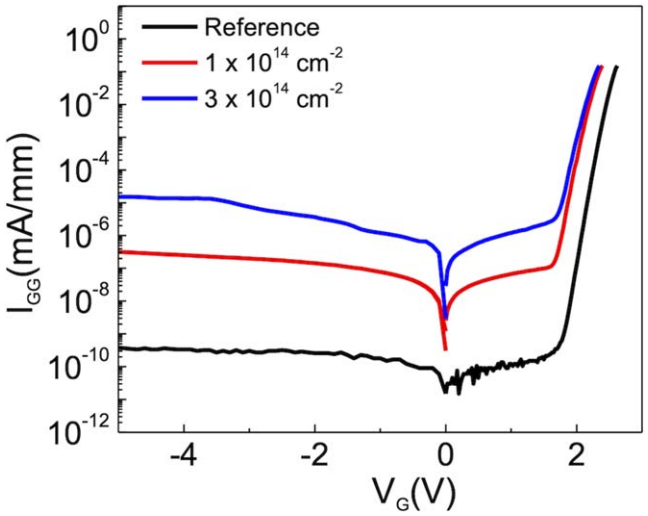

Figure 5. I_{gg}-V_g curves of the reference and irradiated POLFETs.

Table II. Extracted average ideality factor and Schottky barrier heights for POLFETs before and after irradiation.

Sample	n	SBH (eV)
Reference	1.37 ± 0.08	2.21 ± 0.13
Irradiated 1 × 10^{14} cm^{-2}	1.67 ± 0.06	1.79 ± 0.04
Irradiated 3 × 10^{14} cm^{-2}	1.88 ± 0.02	1.62 ± 0.01

shown in Fig. 4, with an average 20.6% ± 1% and 35.8% ± 1.4% reduction in transconductance, g_m. As a positive shift in the threshold voltage is apparent, the carrier density should reflect a similar reduction. Using the following equation, which was derived to describe the carrier density in the two-dimensional electron gas (2DEG) of a GaN HEMT device under strong inversion, we can approximate the change in carrier density.[17]

$$n_s = \frac{2\varepsilon qD}{\varepsilon + 2q^2Dd}(V_{gs} - V_{th}) \quad [3]$$

where ε is the dielectric constant of the barrier layer, V_{gs} is the applied gate to source voltage under strong inversion, V_{th} is the threshold voltage, and D is the conduction band density of states where $D = 4\pi m^*/h^2$, m* is the effective electron mass and h is Planck's constant. The average extracted sheet carrier concentrations for the reference, low dose, and high dose devices are 6.00 ± 0.25 × 10^{12} cm^{-2}, 5.16 ± 0.27 × 10^{12} cm^{-2}, and 4.38 ± 0.51 × 10^{12} cm^{-2}, respectively. While this approximation is not entirely analogous to the POLFET structure, as the current flow is with a 3D electron slab (3DES) rather than a 2DEG, it still can provide a starting point for analysis of the carrier concentration. The reference state extraction compares very well to the extracted carrier concentration by contactless mercury probe CV, 5.4 × 10^{12} cm^{-2}, which affirms the solution obtained. The carrier removal rates were extracted and defined by:

$$R_c = \frac{n_{s0} - n_s}{\Phi} \quad [4]$$

where Φ is the proton fluence, n_{s0} is the initial carrier concentration, and n_s is the irradiated carrier concentration. The values were normalized to volume density via the depth of the 3DES to place them in units of cm^{-1} rather than unitless for comparison to other irradiation works. The average carrier removal rate was calculated to be 677 ± 353 cm^{-1}. This variation can be attributed to variation within the devices due to growth defects. Pearton et al. reported a summary plot which finds for similar energy proton irradiation, GaN HEMT devices underwent similar carrier removal rates to those found here.[8] This is due to fact that while the carrier distribution of the 3DES is spread across a larger depth of the device and there are more potential interactions for protons with the carriers; however, the modeled SRIM interactions in these alloys, Fig. 2, demonstrate the improvements due to bond strength at resisting these damaging interactions.

In the I_d-V_g curves shown in Fig. 4, the leakage current significantly degraded with irradiation, which is due to the change in the gate contacts performance. In Fig. 5, I_{gg}-V_g curves are presented. Using the thermionic emission model, the Schottky Barrier height and ideality factor can be fit to the following:

$$I = I_0 \exp\left(\frac{qV}{nkT}\right)\left[1 - \exp\left(-\frac{qV}{kt}\right)\right] \quad [5]$$

$$I_0 = AA^{**}T^2 \exp\left(-\frac{q\phi_b}{kT}\right) \quad [6]$$

where I_0 is the reverse saturation current, V is the applied voltage, n is the ideality factor, A is effective diode area, A** is the Richardson constant, k is the Boltzmann constant, and ϕ_b is the SBH. The extracted values are presented in Table II. As is consistent with the leakage current, the barrier height demonstrates an average 0.41 ±.08 eV and 0.66 ± 0.07 eV reduction at the doses of 1 × 10^{14} cm^{-2} and 3 × 10^{14} cm^{-2}, respectively. With a reduction in barrier height, the expected shift in threshold voltage is to the negative, but that does not account for changes in charged traps within the graded layer which may shift the threshold to the positive.

Charged traps near the electron channel screen and decrease the carrier concentration. Additionally, the generation of new charged traps can significantly hinder the medium and high frequency operation by carrier scattering from radiation induced defects. To assess the changes under pulsed conditions, the effects of generation of traps and formation of a virtual gate were examined using gate lag measurements performed at 100 kHz and 10%–50% duty. The testing was performed on the POLFET devices alongside SiN_x GaN MISHEMT devices for comparison, as shown in Fig. 6. The POLFET devices, outside of a small reduction in the overall current from a loss of carriers, demonstrate no change in pulsed characteristics, while the GaN HEMT devices' pulsed current is severely degraded. The carrier scattering effects will be much more pronounced within the 2DEG of the GaN HEMT, as the electrons may end up in the buffer or barrier layer. However, in the POLFET device, as the 3DES has a thickness of approximately 55 nm, the scattering events are less likely for the electron to end outside of the channel and not contribute to the forward current. The GaN based devices exhibited the normal trend of smaller pulse width leading to lower current in switching performance, as there is less time for de-trapping of electrons to occur. The POLFET devices exhibited a slight but opposite trend of shorter pulse width giving a higher current. With the device beings switched on for only 1–5 μs and remaining off for 9–5 μs, the device may not have enough time to reach steady state operating temperature. Longer pulse width lead to increased device heating and channel resistance. The increased time to steady state is due to the poor thermal conductivity of the ternary AlGaN alloys, which experience heightened effects of phonon-phonon and point-defect scattering.[18]

Conclusions

The effects of proton irradiation dose were explored on high aluminum content POLFETs with a fixed energy of 10 MeV at doses of 1 × 10^{14} cm^{-2} and 3 × 10^{14} cm^{-2}. As irradiation dose was increased, a parallel reduction in saturation forward current, carrier concentration, and transconductance were noted. While the reduction in barrier height of the Schottky gate lead to an increase in the leakage currents, an opposite shift to the positive for the threshold voltage was noted. This shift can be attributed to the formation of

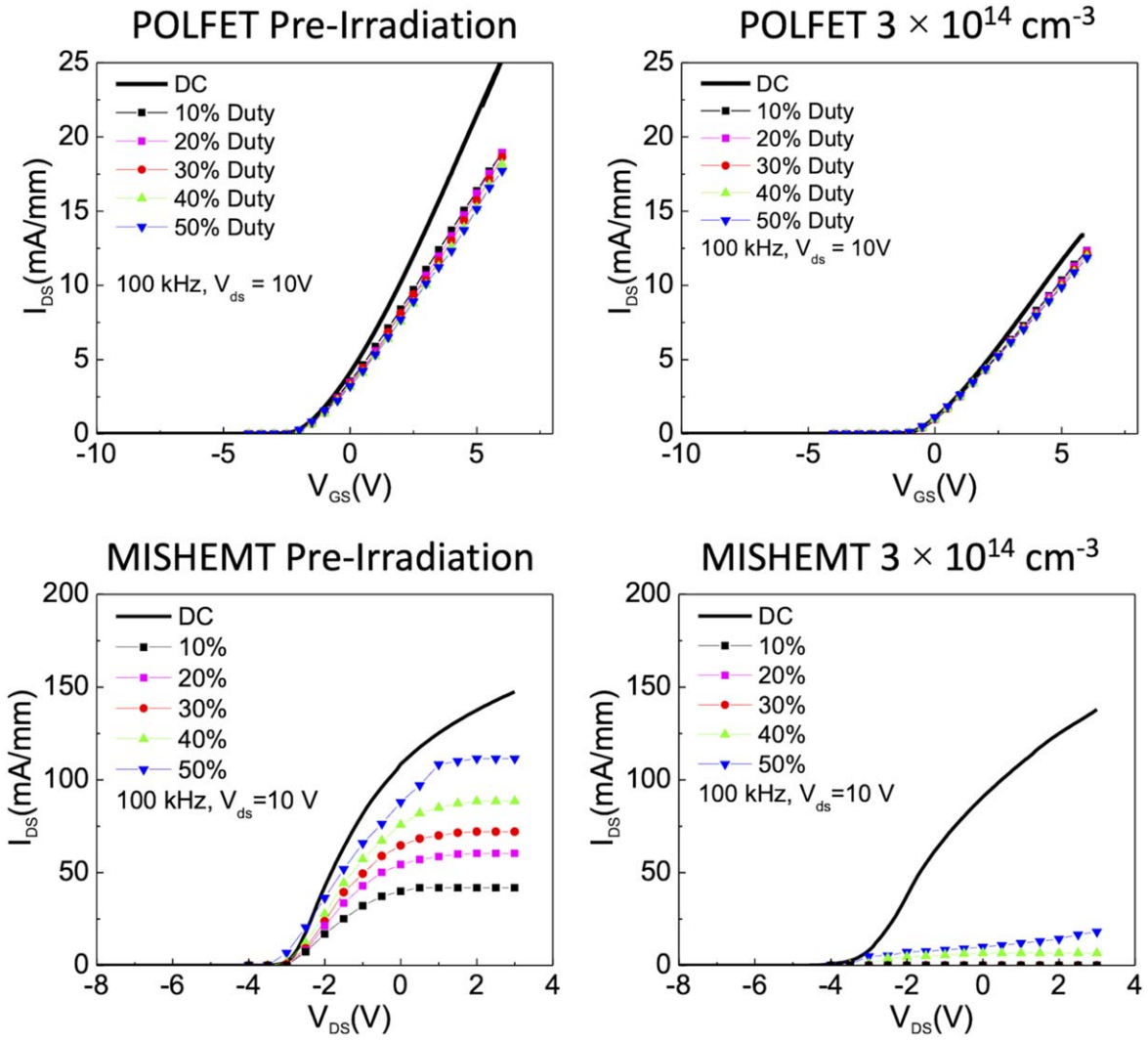

Figure 6. Gate-lag performed at V_{ds} = 10 V and gate switching from V_{gs} = −8 to the data point at 100 kHz with a varied duty cycle from 10 to 50% for POLFETs and traditional SiN_x GaN MISHEMTs.

positive trapped charges within the graded layer. These trapped charges did not have any effect on the 100 kHz switching performance of the devices, as opposed to significant deleterious effect on the GaN based devices. These results demonstrate a positive outlook for high aluminum content POLFETs in extra-terrestrial applications and may extend device lifetime significantly.

Acknowledgments

The work at UF was partially sponsored by the Department of the Defense, Defense Threat Reduction Agency, No. HDTRA1-17-1-011, monitored by Jacob Calkins. The research at Korea University was supported by the National Research Foundation of Korea (2018R1D1A1A09083917) and the Korea Institute of Energy Technology Evaluation and Planning (KETEP) (20172010104830).

ORCID

Patrick H. CareyIV https://orcid.org/0000-0002-8826-3977
Stephen J. Pearton https://orcid.org/0000-0001-6498-1256

References

1. J. A. Van Allen, C. E. McIlwain, and G. H. Ludwig, "Radiation observations with satellite 1958 ε." *J. Geophys. Res.*, **64**, 271 (1959).
2. J. Feynman, G. Spitale, J. Wang, and S. Gabriel, "Interplanetary proton fluence model: JPL 1991." *Journal of Geophysical Research: Space Physics*, **98**, 13281 (1993).
3. T. J. Anderson, A. D. Koehler, J. A. Freitas, B. D. Weaver, J. D. Greenlee, M. J. Tadjer, E. A. Imhoff, K. D. Hobart, and F. J. Kub, "Hyperspectral electroluminescence characterization of OFF-state device characteristics in proton irradiated high voltage AlGaN/GaN HEMTs." *ECS J. Solid State Sci. Technol.*, **5**, Q289 (2016).
4. T. J. Anderson, D. J. Meyer, A. D. Koehler, J. A. Roussos, B. D. Weaver, K. D. Hobart, and F. J. Kub, "Impact of 2 MeV proton irradiation on the large-signal performance of Ka-Band GaN HEMTs." *ECS J. Solid State Sci. Technol.*, **6**, S3110 (2017).
5. C. Fares, F. Ren, S. J. Pearton, G. Yang, J. Kim, C.-F. Lo, and J. W. Johnson, "Effect of proton irradiation energy on SiN_x/AlGaN/GaN metal-insulator semiconductor high electron mobility transistors." *Journal of Vacuum Science & Technology B*, **36**, 052202 (2018).
6. J. C. Gallagher, T. J. Anderson, A. D. Koehler, N. A. Mahadik, A. Nath, B. D. Weaver, K. D. Hobart, and F. J. Kub, "Effect of surface passivation and substrate on proton irradiated AlGaN/GaN HEMT transport properties." *ECS J. Solid State Sci. Technol.*, **6**, S3060 (2017).
7. J. D. Greenlee, P. Specht, T. J. Anderson, A. D. Koehler, B. D. Weaver, M. Luysberg, O. D. Dubon, F. J. Kub, T. R. Weatherford, and K. D. Hobart, "Degradation mechanisms of 2 MeV proton irradiated AlGaN/GaN HEMTs." *Appl. Phys. Lett.*, **107**, 083504 (2015).
8. S. J. Pearton, F. Ren, E. Patrick, M. E. Law, and A. Y. Polyakov, "Review—ionizing radiation damage effects on GaN devices." *ECS J. Solid State Sci. Technol.*, **5**, Q35 (2015).
9. B. D. Weaver, T. J. Anderson, A. D. Koehler, J. D. Greenlee, J. K. Hite, D. I. Shahin, F. J. Kub, and K. D. Hobart, "Editors' choice—on the radiation tolerance of AlGaN/GaN HEMTs." *ECS J. Solid State Sci. Technol.*, **5**, Q208 (2016).
10. S. Bajaj et al., "High Al-content AlGaN transistor with 0.5 A/mm current density and lateral breakdown field exceeding 3.6 MV/cm." *IEEE Electron Device Lett.*, **39**, 256–59 (2018).

11. P. H. Carey IV, F. Ren, A. G. Baca, B. A. Klein, A. A. Allerman, A. M. Armstrong, E. A. Douglas, R. J. Kaplar, P. G. Kotula, and S. J. Pearton, "Operation up to 500 ° C of $Al_{0.85}Ga_{0.15}N/Al_{0.7}Ga_{0.3}N$ high electron mobility transistors." *IEEE J. Electron Devices Soc.*, **7**, 444–52 (2019), 10.1109/JEDS..29073062019.
12. E. A. Douglas, S. Reza, C. Sanchez, D. Koleske, A. Allerman, B. Klein, A. M. Armstrong, R. J. Kaplar, and A. G. Baca, "Ohmic contacts to Al-rich AlGaN heterostructures." *Physica Status Solidi (a)*, **214**, 1600842 (2017).
13. Y. Zhang and J. Singh, "Charge control and mobility studies for an AlGaN/GaN high electron mobility transistor." *J. Appl. Phys.*, **85**, 587 (1999).
14. J. Simon, V. Protasenko, C. Lian, H. Xing, and D. Jena, "Polarization-induced hole doping in wide-band-gap uniaxial semiconductor heterostructures." *Science*, **327**, 60 (2010).
15. A. M. Armstrong, B. A. Klein, A. Colon, A. A. Allerman, E. A. Douglas, A. G. Baca, T. R. Fortune, V. M. Abate, S. Bajaj, and S. Rajan, "Ultra-wide band gap AlGaN polarization-doped field effect transistor." *Jpn. J. Appl. Phys.*, **57**, 074103 (2018).
16. M. J. Martinez, M. P. King, A. G. Baca, A. A. Allerman, A. A. Armstrong, B. A. Klein, E. A. Douglas, and R. J. Kaplar, "Radiation response of AlGaN-channel HEMTs." *IEEE Trans. Nucl. Sci.*, **66**, 344 (2019).
17. A. Rashmi, S. Kranti, Haldar, and R. S. Gupta, "An accurate charge control model for spontaneous and piezoelectric polarization dependent two-dimensional electron gas sheet charge density of lattice-mismatched AlGaN/GaN HEMTs." *Solid-State Electronics*, **46**, 621 (2002).
18. W. Liu and A. A. Balandin, "Thermal conduction in $Al_xGa_{1-x}N$ alloys and thin films." *J. Appl. Phys.*, **97**, 073710 (2005).